Llavori, I.; Giner Maravilla, E.; Zabala, A.; Infante, D.; Aginagalde, A.; Rodríguez-Flórez, N.; Gómez, X. (2019). Critical analysis of the suitability of crack propagation direction criteria for 2D cylindrical plain fretting contact. Engineering Fracture Mechanics. 214:534-543. https://doi.org/10.1016/j.engfracmech.2019.04.035

Critical analysis of the suitability of crack propagation direction criteria for 2D cylindrical plain fretting contact

I. Llavori[1,*], E. Giner[2], A. Zabala[1], D. Infante-Garcia[3], A. Aginagalde[1], N. Rodríguez-Flórez[1], X. Gómez[1]

[1] Surface Technologies, Mondragon University, Loramendi 4, 20500 Arrasate-Mondragon, Spain.

[2] Centre of Research in Mechanical Engineering - CIIM, Dept. of Mechanical Engineering and Materials, Universitat Politècnica de València, Camino de Vera, 46022 Valencia, Spain.

[3] Dept. of Mechanical Engineering, University Carlos III of Madrid, Avda. de la Universidad 30, 28911 Leganes, Madrid, Spain.

*Corresponding author: Iñigo Llavori, illavori@mondragon.edu

Journal: *Engineering fracture mechanics*

Abstract

In this work the suitability of the criterion of maximum effective amplitude of the normal stress $(\Delta\sigma_{n,eff})_{max}$ and the criterion of minimum shear stress range $(\Delta\tau)_{min}$ for 2D cylindrical plain fretting contact condition has been analysed. The numerical analysis has been performed by means of the extended finite element method, which takes into account the contact between crack faces during the closing part, and the results have been compared with experiments reported in the literature. **Results show that overall the $(\Delta\tau)_{min}$ criterion predominates in intermediate stage, while the $(\Delta\sigma_{n,eff})_{max}$ shows less deviation in the final stage. However, the predicted crack path by the latter criterion shifts toward the outer side, which do not correlate with the experimental results reported in the literature.** Additional studies should investigate the variables that are affecting this change in the behaviour along the crack in order to set a criteria that is able to predict the plain fretting condition crack paths accurately.

Key words: Crack paths, Crack propagation, Fretting, Extend finite elements

Nomenclature

FEA	Finite Element Analysis

FIP	Fatigue Indicator Parameters
LSM	Level Set Method
MPC	MultiPoint Constraints
MTS	**Maximum Tangential Stress**
PUM	Partition of Unity Method
SIF	Stress Intensity Factors
SWT	Smith-Watson-Topper
X-FEM	eXtended Finite Element Method
$\mathbf{a}_i$,	Degrees of freedom of the Heaviside enriched nodes
$\mathbf{b}_i^l$	Degrees of freedom of the crack tip enriched nodes
$b_{\mathrm{p,CA}}$	Maximum projected crack length related to the crack arrest condition
E	Young's modulus
e_{path}	Average deviation of the crack path
$H(\mathbf{x})$	Heaviside step function
L_i	Crack length of the segment i
$N_i(\mathbf{x})$	Conventional nodal shape function
P	Fretting contact force
Q	Fretting tangential force
$\mathbf{u}_i$	Classical degree of freedom of the FEM
$x_{\mathrm{predicted}}$	x coordinate at each y coordinate of the predicted numerical path
$x_{\mathrm{exp.\ path}}$	x coordinate at each y coordinate of the experimental path

Greek letters

$(\Delta\sigma_{\mathrm{n,eff}})_{\mathrm{max}}$	The criterion of the maximum amplitude of the normal stress
$(\Delta\tau)_{\mathrm{min}}$	The criterion of minimum shear stress range
ΔK_{th}	Threshold value of the SIF
ν	Poisson coefficient
θ_i	Angle i with the normal plane of the surface
σ_{n}	Normal stress
σ_{Y}	Yielding stress
σ_{u}	Ultimate stress
σ_{e}	Endurance limit

σ_∞	Cyclic bulk stress
μ_t	Coefficient of frictionat the sliding transition

1.-Introduction

Fretting problems arise when two contacting bodies are subjected to movements of small relative displacement (0-300 microns) promoting micro-cracks and eventually the failure of the component [1]. Fretting is reported commonly in the industry since virtually all machines vibrate, and failure can occur in many mechanical components such us flexible couplings, aircraft engine blade housings, lug joints or ropes.

Fretting fatigue lifetime prediction is an object of interest in the fatigue community. Usually, the study is divided into two phases, the crack nucleation and crack propagation. One crucial step in order to give a robust fatigue life estimation is hence the correct crack path prediction, which is the focus of the present work.

Propagation phase is usually divided into 3 stages as shown in **Fig. 1** [2]. **Crack growth in stage I is dominated by shear stress, leading to a crack path direction towards the inner zone of the contact. This stage is also known as the crack incubation stage [3, 4, 5] where the accumulated damage is related to the permanent plastic deformation of the material. Different approaches have been used to study crack initiation, such as multiaxial fatigue parameters [6, 7, 8, 9], continuum damage mechanics [10, 11], or crystal plasticity [12, 13]. Bhatti and Wahab recently published an exhaustive literature review discussing the different approaches [14]. Regarding stage II on propagation stage, the shear stress produced by the contact is less pronounced and a mixed tensile and shear stress field is observed. Therefore, crack growth tends to change towards a more vertical direction. In stage III the effect of the contact is even less pronounced and consequently, the propagation is assumed to happen in mode I. (*i.e.* tensile stress dominated and governed by the remote cyclic stress σ_∞). The number of cycles for crack initiation is greatly influenced by the type of contact. The crack initiation period is reported to be very short in complete contacts [15], whereas it is usually longer in incomplete contacts [10]. Regarding the following propagation stages, it should be highlighted the predominance contribution of the stage II, since the crack grows slower compared to stage III. It should be noted that in plain fretting tests crack arrest conditions are achieved in the absence of a remote cyclic stress.**

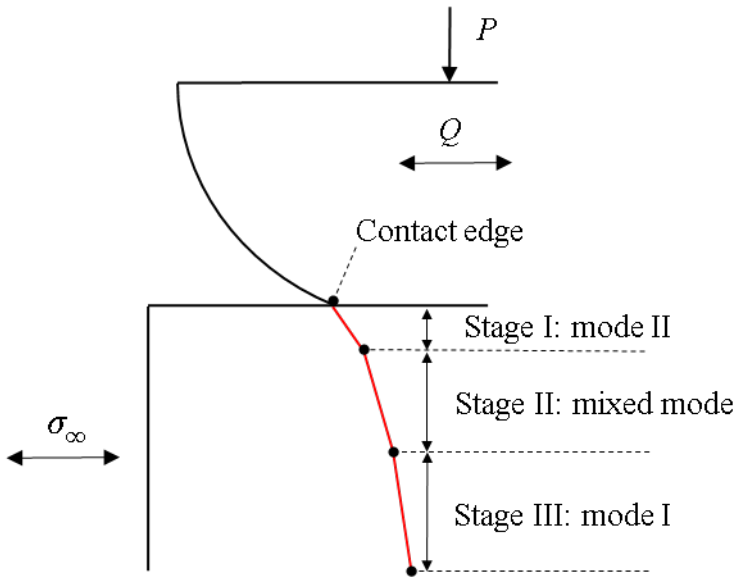

Fig. 1. Sketch of the 3 stages of propagation in fretting.

Many crack direction models have been developed throughout history aimed at predicting the orientation of the crack [16, 17, 18, 19, 20, 21]. Those models can be broadly classified into two main categories, namely, (i) proportional loading models, and (ii) non-proportional loading models. Fretting fatigue is characterised with a highly non-linear and non-proportional evolution of stresses along the contact zone. Accordingly, proportional models are not valid and only the non-proportional ones should be used. Among the non-proportional models, some criteria are based on fracture mechanics, where the analysis of the stress intensity factors (SIF) are the driving parameters, whereas other models are based on the stress field analysis. Dubourg and Lamacq [19] proposed the criterion of the maximum amplitude of the normal stress $(\Delta\sigma_{n,eff})_{max}$ for a cylindrical contact, although the experiment was based on spherical contact. Nevertheless, the predicted crack path was in good agreement with the experiment. Giner *et al*. [21] reviewed several non-proportional criteria relevant to the fretting fatigue phenomenon, highlighting that the computation of the K_{II} values under non-proportional crack face contact are cumbersome and prone to inaccuracies when using domain and contour integrals, although it should be mentioned that good results have been published [20, 22]. Giner *et al*. [21] tested the $(\Delta\sigma_{n,eff})_{max}$ criterion for fretting fatigue flat contacts and showed that results were not in good agreement with the experimental observations. Consequently, they proposed an equivalent to the so-called "criterion of local symmetry" for non-proportional loading, which seeks the path that minimises the shear stress range at a point ahead of the crack tip. This approach was validated for fretting fatigue flat contact configuration and later on was used by Martínez *et al*. [23] to predict the crack path in a railway axle (flat on flat contact), obtaining a good agreement with the experimental result. Conversely, Cardoso *et al*. [24] found that the prediction may lead to wrong paths for fretting fatigue cylindrical contact configuration.

Recently, Navarro *et al.* [25] compared the capability of some fatigue indicator parameters (FIP) to predict the crack initiation path. They pointed out that although using FIPs based on the critical plane approach is not correct, the concept of the damage could be related, based on the fact that the predicted paths of the Smith-Watson-Topper (*SWT*) parameter were very similar to the experiments.

Following the concept of the stress field analysis used by Dubourg and Lamacq [19] and Giner *et al*. [21], the present work aims at evaluating the accuracy of different crack orientation criteria for plain fretting in 2D cylindrical contacts using the eXtended finite element method (X-FEM) code for Abaqus FEA. The numerical results are compared to experimental data reported in the literature.

2.- Crack direction criteria for non-proportional loading

As stated by Socie and Marquis [26], "*Depending on the material, stress state, environment, and strain amplitude, fatigue life usually will be dominated by crack growth along either shear planes or tensile planes*". Accordingly, in this work the crack growth paths have been modelled following tensile and shear criteria, namely, the maximum effective amplitude of the normal stress (tensile driven criterion), and the minimum shear stress range (shear driven criterion).

2.1 The criterion of maximum effective amplitude of the normal stress

The first criterion selected is the maximum effective amplitude of the normal stress $(\Delta\sigma_{n,eff})_{max}$ proposed by Dubourg and Lamacq [19], which is an extension of the well known **maximum tangential stress** (MTS) criterion [16] for non-proportional loading. The results of Dubourg and Lamacq pointed out the importance of considering the range of the stresses rather than taking only the maximum values. Therefore, this criterion is based on the concept that the crack growth is dominated by the effective maximum amplitude of the normal stress of crack opening. Accordingly, the term effective considers that $\sigma_n=0$ when $\sigma_n<0$, which means that the compressive part of the cycle (*i.e.* during crack-face contact) is not considered in this criterion (see **Fig. 2**) . **Therefore, the criterion cannot fully consider the non-proportional loading effect, which could be very important as shown in the literature [21].**

One of the main weaknesses of the criterion is that many candidate planes coexist near the maximum value identified. As observed in **Fig. 2**, the maximum value of the $\Delta\sigma_{n,eff}$ is nearly the same for the planes ranging between **0-20º and** 160-180º, which makes it difficult to robustly define the propagation plane.

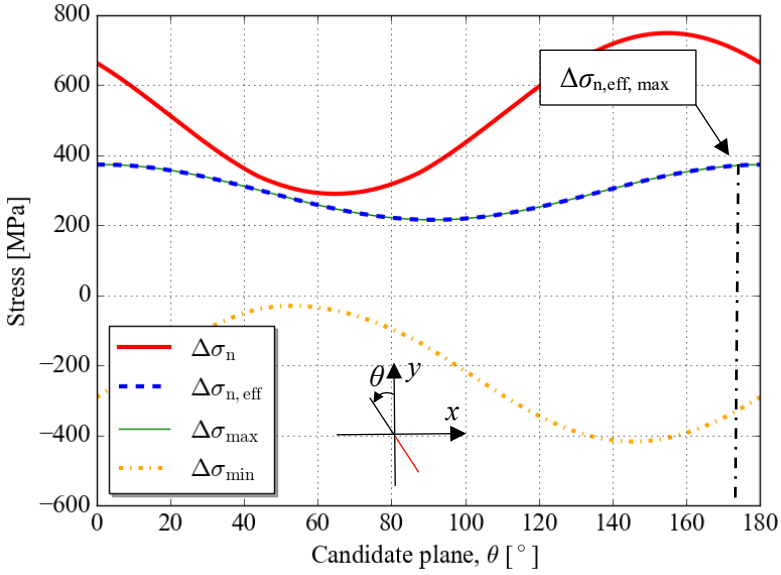

Fig. 2. Criterion of the maximum effective amplitude of the normal stress $\Delta\sigma_{n,eff}$.

2.2 The criterion of minimum shear stress range

As stated on the introduction, the criterion proposed by Giner *et al*. [21] was a generalization for non-proportional loading of the "criterion of local symmetry" proposed by Cotterell and Rice [27]. This criterion assumes that the crack will propagate in the direction of pure mode I ($K_{II} = 0$). Due to the non-proportionality in fretting, this condition cannot be reached, so the $(\Delta\tau)_{min}$ criterion seeks to find the plane where the loss of friction energy is minimal (*i.e*, the plane that is closer to pure mode I condition). Given the nature of shear stresses (see **Fig. 3**), two orthogonal planes with the minimum value coexist, and the direction of propagation is defined as the one that is subjected to the highest range of normal stress ($\Delta\sigma_{n\,1}$).

In contrast to the previously introduced $\Delta\sigma_{n,eff}$ criterion, the $(\Delta\tau)_{min}$ criterion considers the full fretting cycle including the compressive part, and presents the advantage of being a robuster method, since the curve is sharper near the lowest value and therefore, the propagation candidate plane is clearly identified. Physically, this can be linked to a well defined propagation direction, as often observed in practice. A larger scatter would be expected experimentally for prospective directions close to the direction of maximum $\Delta\sigma_{n,eff}$ if the latter were the criterion governing crack orientation.

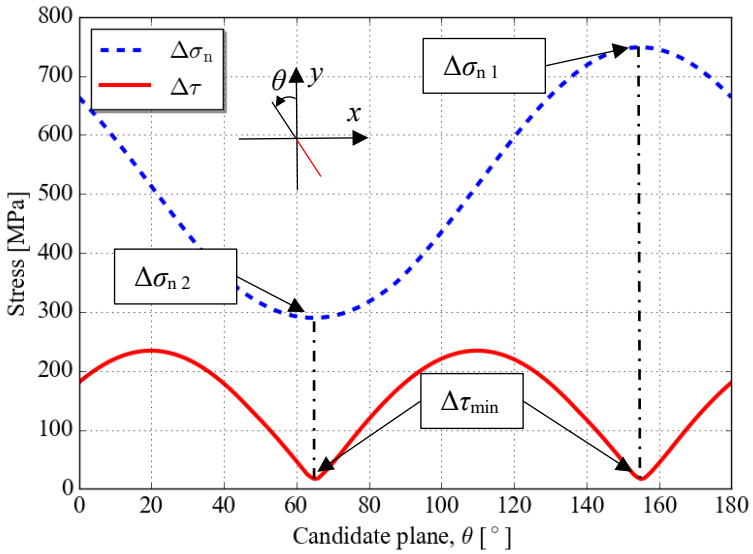

Fig. 3. Criterion of the minimum shear stress range $\Delta\tau_{min}$. $\Delta\sigma_{n\,1,2}$ refer to normal stresses.

3.- Experimental tests from the literature

Plain fretting experimental tests reported by Pannemaecker *et al*. [28] were used for numerical result comparison. These tests were performed under a stick-slip regime, where a constant normal force P and a reciprocating cyclic displacement were applied.

Due to the cyclic stress-strain, a crack in the edge of the contact was nucleated and propagated until approximately 10^6 cycles, where the crack arrest condition was achieved. **Fig. 4** shows the typical crack path obtained in these tests, which was simplified through three segments (L_1, L_2, and L_3) and the corresponding angles (θ_1, θ_2, and θ_3). The reader is referred to Pannemaecker's article [28] for further details on these experimental crack paths.

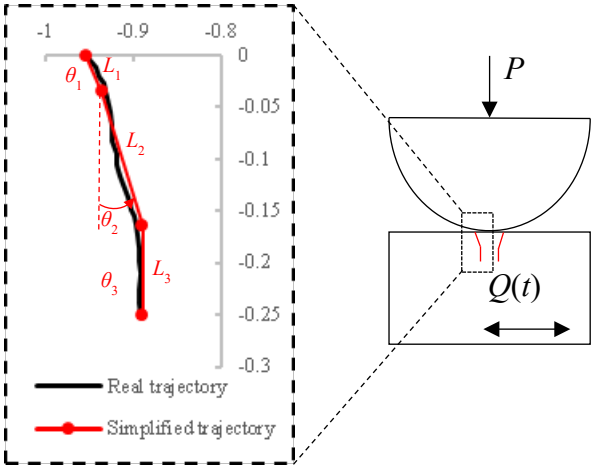

Fig. 4. Analysis of the crack path in Pannemackers's test number 11 [28].

The selected tests from [28] correspond to the ones performed with Ti-6Al-4V cylindrical pads and Al7075-T6 flat specimens. The used material shows high yield strength with respect to the ultimate tensile strength, making it suitable for linear elastic fracture mechanics (LEFM) analysis (mechanical properties are presented in **Table 1**). Additionally, this material configuration (being the titanium indenter of higher strength) ensures that the crack initiates only on the flat aluminium specimen. In all these tests the radius of the cylindrical pad and the contact force were kept constant, R = 80 mm and P = 461 N/mm (force per unit thickness) respectively, while the tangential force Q was changed in each test (details presented in **Table 2**).

Table 1. Mechanical, fatigue and fracture properties taken from Pannemaecker *et al*. [28].

Material	E [GPa]	ν [-]	σ_Y [MPa]	σ_u [MPa]	σ_e [MPa]	ΔK_{th} [MPa m$^{0.5}$]
Al7075-T6	70	0.33	520	575	150	3.72
Ti-6Al-4V	119.5	0.287	970	1100	-	-

Table 2. Elastic test conditions and related analysis of crack arrest conditions taken from Pannemaecker *et al*. [28]. * *Note that the test presentation order has been changed from the original paper, ordering from the lowest (Test 11/ renamed as Test A) to the highest Q force (Test 7 / renamed as Test F).*

Test	A	B	C	D	E	F
(*Original numbering*)	*11*	*8*	*10*	*9*	*12*	*7*
Q (N/mm)	260	299	313	334	341	350
μ ratio	0.74	0.72	0.56	0.68	0.56	0.65

μ_t	1.17	1.17	1.17	1.17	1.17	1.17
$b_{p,CA}$ (μm)	217	261	416	524	495	750
L_1 (μm)	38	35	42	49	46	50
θ_1(°)	23	30	45	45	40	5
L_2 (μm)	138	78	102	112	145	221
θ_2(°)	20	20	10	20	15	15
L_3 (μm)	87	156	286	384	355	530
θ_3(°)	0	0	0	0	0	0

4.- Numerical modelling

In this work the X-FEM code for Abaqus FEA developed by Giner *et al*. [29] which incorporates crack face contact capabilities has been used. **The X-FEM approximation to the displacement field $\mathbf{u}^{\text{X-FEM}}(\mathbf{x})$ is defined as:**

$$\mathbf{u}^{\text{X-FEM}}(\mathbf{x}) = \sum_{i\in I} \mathbf{u}_i N_i(\mathbf{x}) + \sum_{i\in L} \mathbf{a}_i N_i(\mathbf{x}) H(\mathbf{x}) + \sum_{i\in K} N_i(\mathbf{x}) \left(\sum_{l=1}^{4} \mathbf{b}_i^l F^l(\mathbf{x}) \right). \quad \text{(Eq. 1)}$$

4.1 Finite element model

The model shown in **Fig. 5** has been developed in the commercial code Abaqus FEA 6.13.1. The linear elastic constitutive model consists of linear quadrilateral elements of 4 nodes (CPE4), with further refinement on the contact area by means of the partition technique. **A convergence study was performed to ensure that the numerical model correctly captures the crack propagation paths. Using element sizes of 5 μm and 10 μm lead both to the same crack path prediction. Therefore, an element size of 10 μm was used in the numerical model.** In order to obtain a precise slip distribution, the Coulomb and the Lagrange multiplier methods have been used to model the tangential contact. The normal force (P) is applied by means of MultiPoint Constraints (MPC).

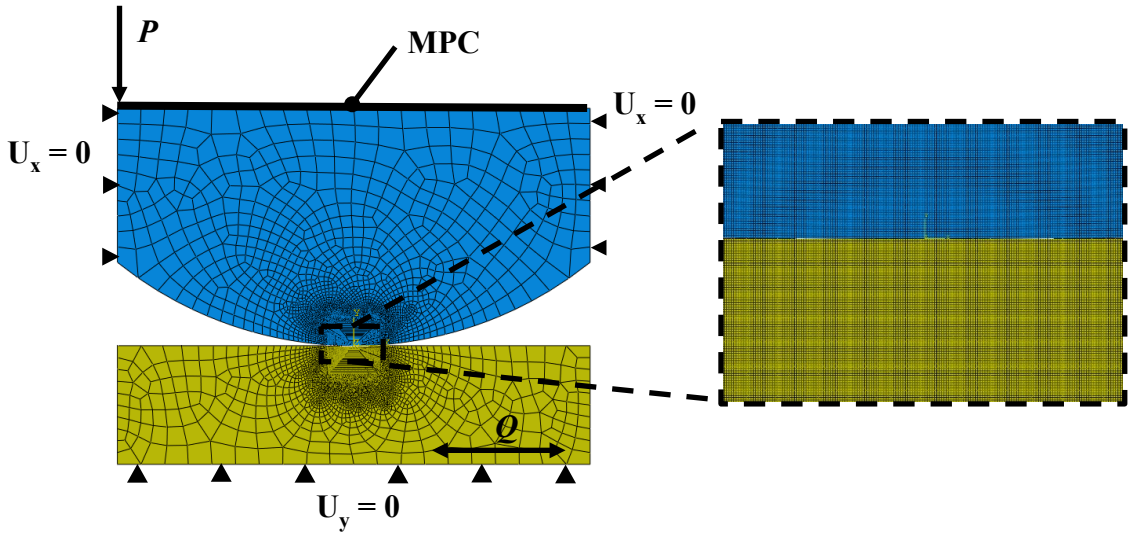

Fig. 5. Geometry, mesh, and applied boundary conditions and forces of the numerical models. *Q* and *P* refer to forces, MPC are multi point constraints and $U_{x,y}$ are displacements in x and y direction respectively.

Fig. 6a shows the load cycle history which has been divided into 3 steps. In the first step, a normal load *P* is applied, followed by a prescribed *Q* force (step 2) in order to accommodate the contacting interface. Finally, a cyclic *Q* (*t*) is applied (step 3), and the crack path is calculated through post-processing at the end of the cycle. This process is repeated until the final length of the crack is achieved. **Fig. 6b** shows a detailed area of the crack and **Figs. 6c-d** plot different increment stages of the cyclic *Q* step, corresponding to the 20, 40 and 60 simulation increments.

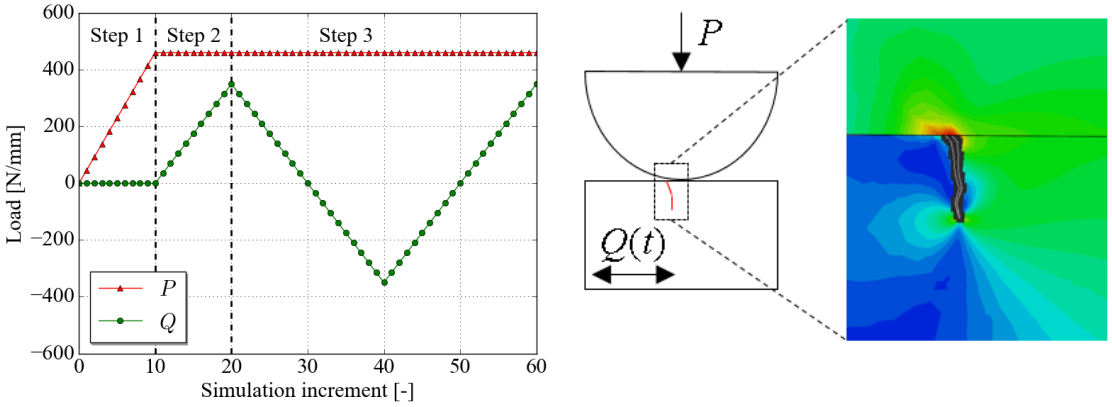

(a) (b)

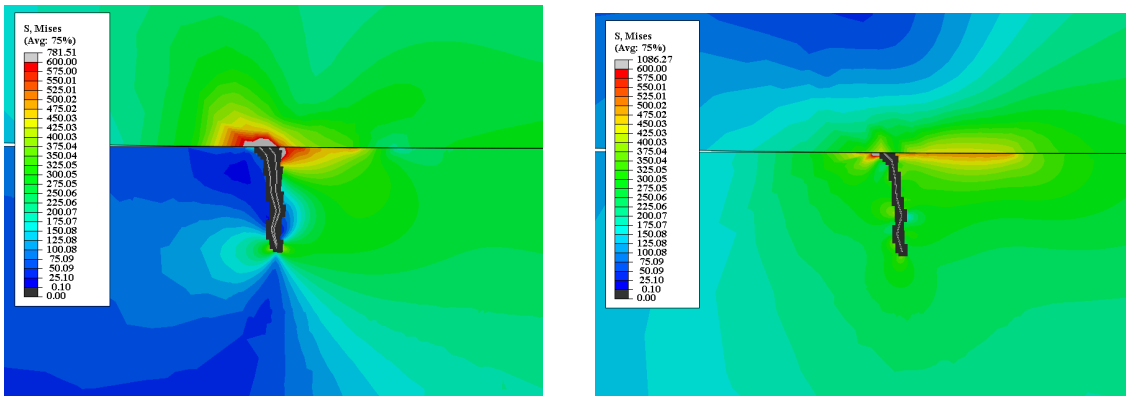

(c) (d)

Fig. 6. Numerical results of the von Mises stress distribution at different stages: (a) load cycle history; (b) detailed area of the cracked zone; (c) Increment 20 and 60, opening of the crack; (d) Increment 40, closure of the crack.

4.2 Stress field analysis ahead of the crack tip

The evaluation of the orientation criteria is carried out ahead of the crack tip. Stresses are computed at the integration points of the element ahead of the crack tip (**Fig. 7**) and averaged to improve the estimation. Averaging is important since the FE discretization error is large in the vicinity of the crack tip. **Several options have been considered, such as averaging stresses at the integration points within a circle of a given radius or analysing the stresses at the centroid of the element. A sensitivity analysis was performed regarding this averaging region (*i.e.* changing the size of the radius). We conclude that differences in the direction estimation were not large, since the estimation of the orientation angle is related to a simple coordinate transformation of stresses to apply the criteria explained in Section 2.**

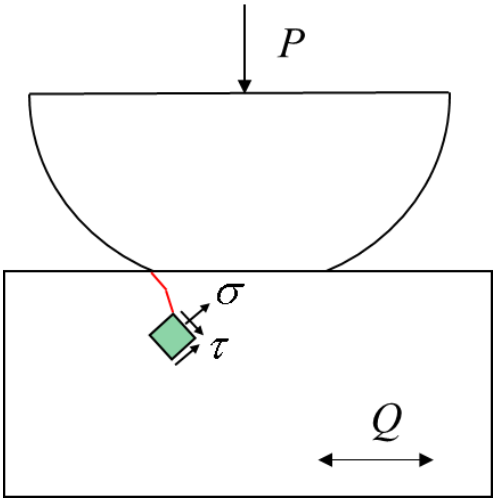

Fig. 7. Sketch of the stress evaluation ahead of the crack tip.

4.3 Crack path prediction accuracy analysis

In order to calculate an indicator of the accuracy of the predicted direction, **a normalised deviation** of the crack path (e_{path}) was calculated as follows:

$$e_{\text{path}} = \int_0^{b_{p.CA}} \left| x_{\text{predicted}} - x_{\text{exp. path}} \right| \mathrm{d}y \Big/ \sum_{i=1}^{3} L_i \,, \qquad \text{(Eq. 3)}$$

where $x_{\text{predicted}}$ and $x_{\text{exp. path}}$ are the x coordinate at each y coordinate of the predicted (numerical) and **the experimental paths**, respectively, and $b_{\text{p,CA}}$ is the projected crack length. The experimental path is approximated to the simplified trajectory through the three segments L_1, L_2 and L_3 shown in Fig. 4 and reported in Table 2 for each case.

5.- Results and discussion

Fig. 8 shows the obtained results, where the predictions of $(\Delta\sigma_{\text{n,eff}})_{\max}$ and $(\Delta\tau)_{\min}$ are depicted along with the experimental observation for the different test conditions. It should be remarked at this point that the present work is aimed at determining the direction of the propagation phase. Accordingly, an initial crack related to the experimental L_1 segment with an angle θ_1 was introduced (the reader is referred to **Fig. 4** and **Table 2** for L_1-θ_1 values) and the comparison of the criteria is therefore carried out only for the L_2-θ_2 and L_3-θ_3 segments.

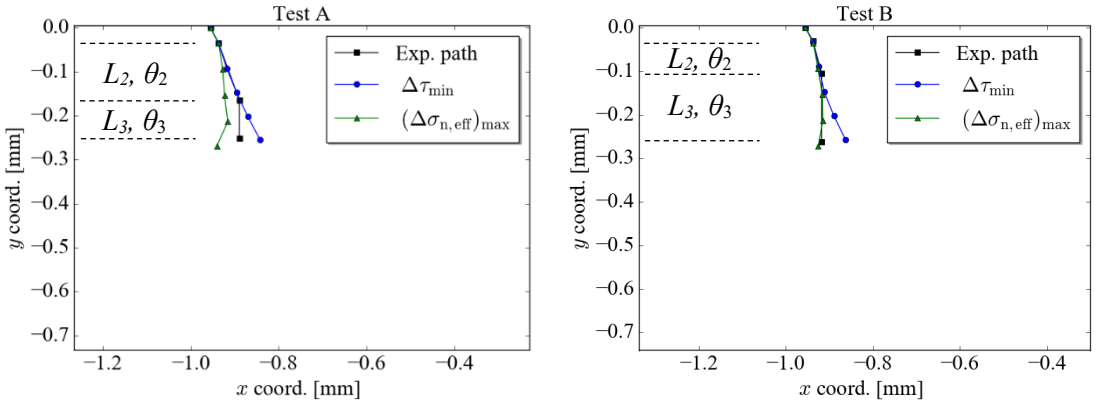

(a) (b)

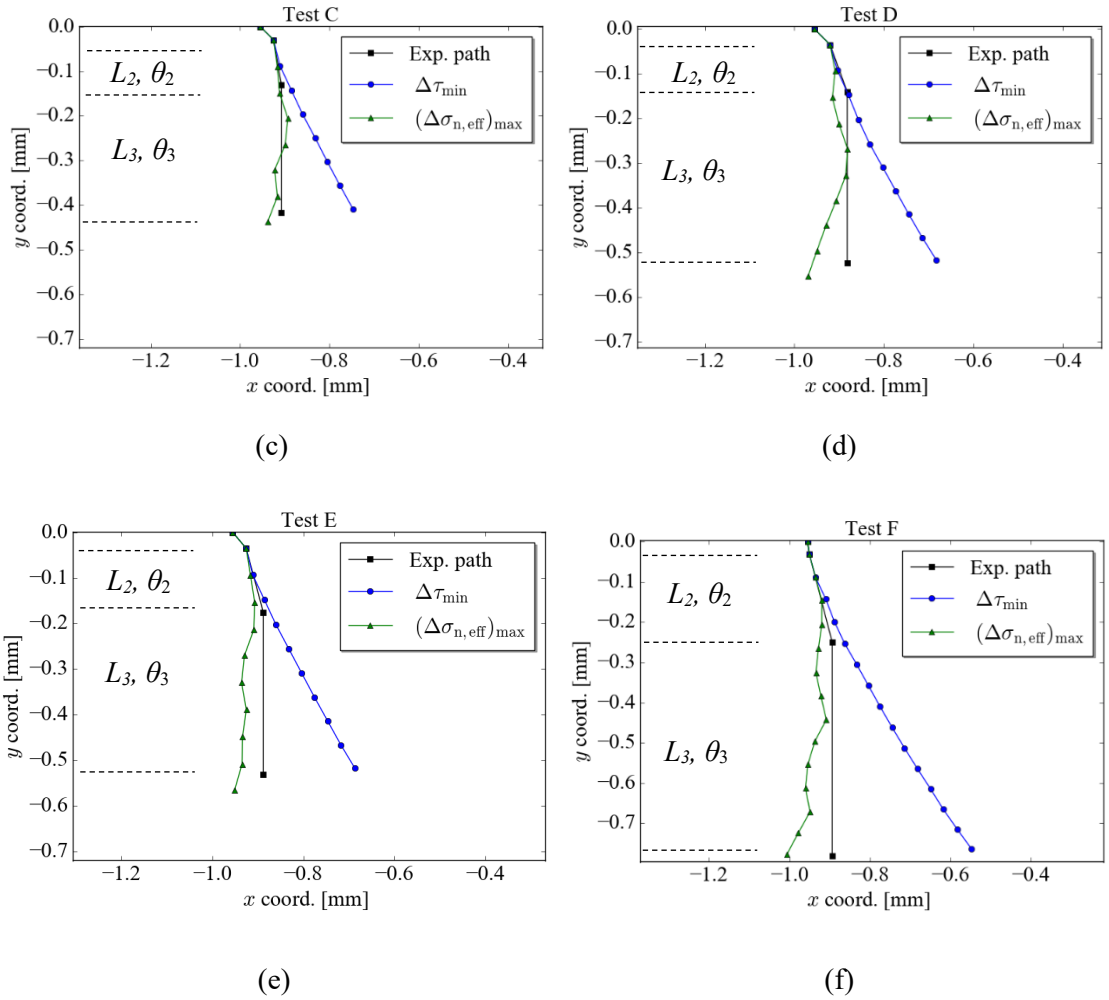

Fig. 8. Predicted crack paths for the selected crack direction criteria and comparison with the experimental paths under different test conditions.

The accuracy analysis has been split into the experimentally identified segments (L_2, and L_2+L_3), in order to identify trends on the numerical prediction. **Fig. 9** shows the average deviation of the predicted crack path by each criterion corresponding to the L_2-θ_2 segment. It can be observed that for the tests ranging from A-E, the $(\Delta\tau)_{min}$ criterion shows a low average deviation (less than 4 μm), proving to be overall the most accurate criterion. Conversely, test C and F present a better correlation for the $(\Delta\sigma_{n,eff})_{max}$ criterion, especially for the test F, which presents a greater average deviation for the $(\Delta\tau)_{min}$ criterion (~10 μm) than for the $(\Delta\sigma_{n,eff})_{max}$ (~6 μm).

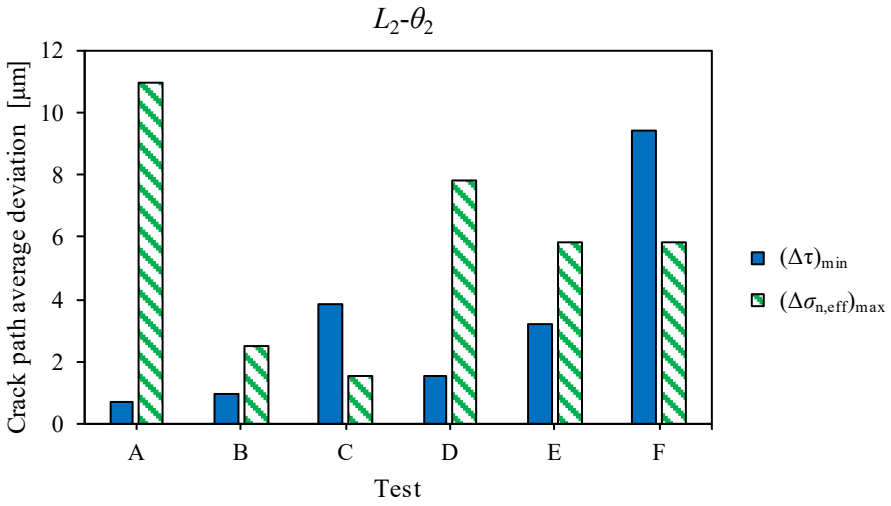

Fig. 9. Average deviation of the selected crack direction criteria at the end of L_2-θ_2 segment.

One of the differences among the two criteria under analysis is the fact that the $(\Delta\sigma_{n,eff})_{max}$ neglects the crack closure events, whereas the $(\Delta\tau)_{min}$ considers the whole cycle. As can be seen in **Fig. 10**, where the time evolution along a cycle of the stress components σ_{xx} and τ_{xy} at the end of each L_i-θ_i segment of test E is shown, the crack is closed (σ_{xx}<0) during approximately half of the fretting cycle. Similar trends are observed in all A-F tests. Consequently, the fact that four of the six cracks are better predicted by the $\Delta\tau$ criteria in the second segment indicates that the crack face contact might be significant and that the shear stress during the closing part has an important role in the propagation path.

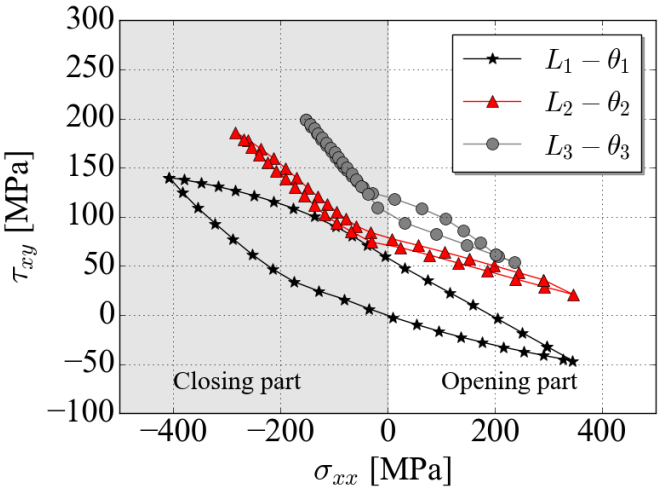

Fig. 10. Evolution of the σ_{xx} and τ_{xy} at the end of each L_i-θ_i segment of test E. Similar trends are observed in the rest

It should be noted that the F test (which showed a big average deviation for the $(\Delta\tau)_{min}$ prediction) presents an almost vertical initial crack ($\theta_1 = 5^o$). In this segment, the maximum shear stress is about 20% lower in the closing part than in test E, while the applied tangential force is higher. Consequently, the ensuing propagation might be less dominated by the shear stress existing during the crack face contact loading part. In this case, the $(\Delta\sigma_{n,eff})_{max}$ shows a lower error (~6 μm) which indicates that the opening part of the crack could dominate the crack growth direction.

Fig. 11 shows the average deviation of the predicted crack path by each criterion at the end of L_3-θ_3 segment. It can be seen that the $(\Delta\sigma_{n,eff})_{max}$ criterion overall predicts a crack path with substantially lower average deviation that the $(\Delta\tau)_{min}$ criterion and that the average deviation obtained by the $(\Delta\tau)_{min}$ criterion increases for higher Q values. It should be mentioned that one of the limitations of the study arises from the fact that the experimental data is based on previously reported literature. One cause of the discrepancies of the $(\Delta\tau)_{min}$ criterion for the last stage may be that the crack paths reported by Pannemaecker *et al*. [28] are simplified to just three segments, being the last always normal to the surface. Further experimental results under similar test conditions are necessary to corroborate these results.

Notwithstanding, the presented results are considered to be a robust comparison since the observed behaviours are consistent with the literature. As previously reported [2] a large scatter in the orientation direction is observed for cracks that have grown substantially. In fact, when the crack is approaching the crack arrest condition, the crack driving force is low and other effects like crack microstructure might have significant influence (see Fig. 6 of reference [2], where it is clearly shown that the grain boundary has an important effect). Another point to consider is the absence of alternating bulk stress that generates cyclic principal stresses parallel to the surface in this region to promote a well defined crack growth in this direction.

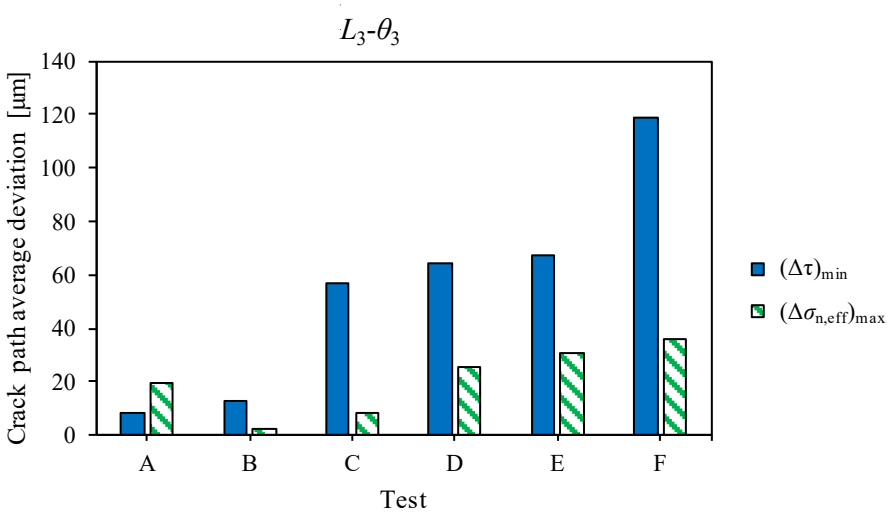

Fig. 11. Average deviation of the selected crack direction criteria at the end of L_3-θ_3 segment.

It should be also highlighted that overall, the $(\Delta\sigma_{n,eff})_{max}$ criteria presents a zigzag path prediction. This is considered an important drawback, since it presents strong implications in terms of crack propagation speed (the pathway travelled could be significantly different than the real one, hence it might overestimate the time needed for the crack to propagate). **Additionally, the prediction obtained by $(\Delta\sigma_{n,eff})_{max}$ criterion overall shifts to the left hand side in stage III, which is not in good agreement with the reported experimental results. This could be related to the erratic behaviour of the $(\Delta\sigma_{n,eff})_{max}$ criterion.**

With the aim of analysing the robustness of each criteria, the distributions of $\Delta\sigma_{n,eff}$ and $\Delta\tau$ (the candidate planes window corresponding to the 10% of the max-min range respectively shown with arrows) are depicted for the three L_i-θ_i segments of test E in **Fig. 12**. As can be observed, the $(\Delta\sigma_{n,eff})_{max}$ criterion presents a less defined target value, with a lot of candidate planes near the target value, which could be the source of the erratic behaviour observed in the predictions. Conversely, the target $(\Delta\tau)_{min}$ value is more clearly defined, showing therefore a more robust candidate plane and consequently an smooth predicted crack path.

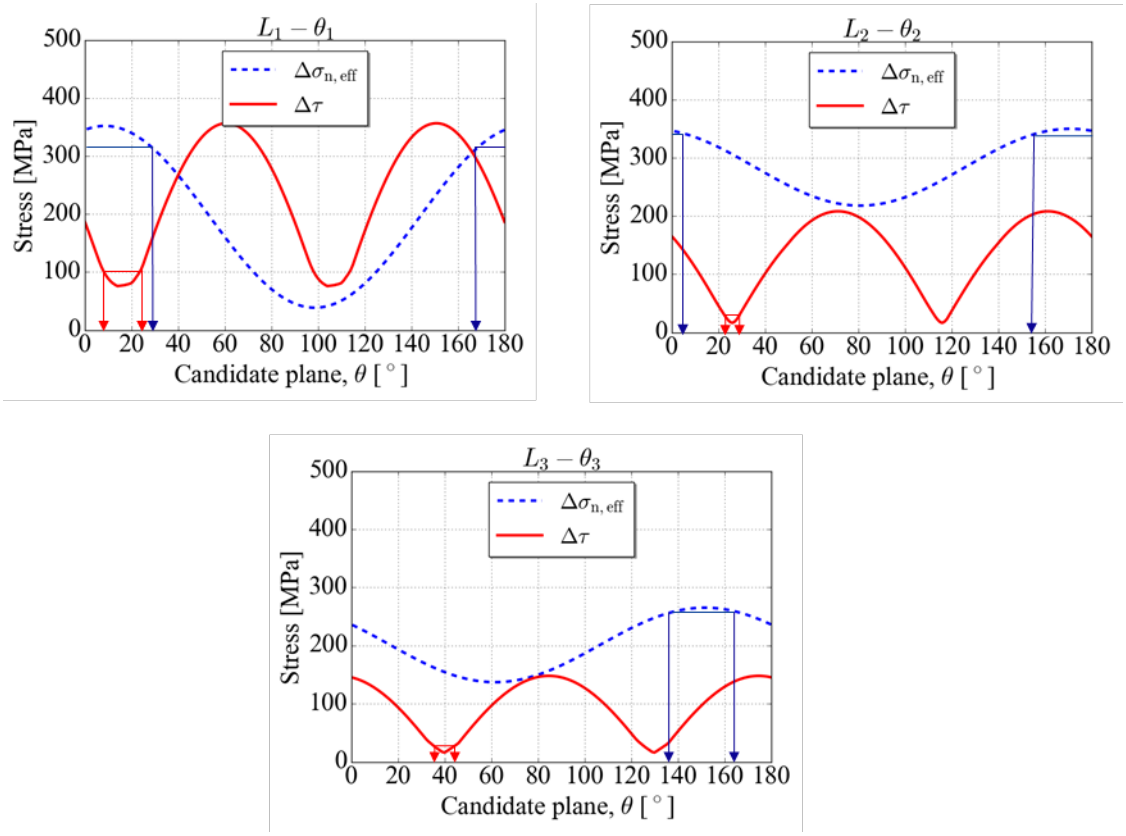

Fig. 12. Comparison between $(\Delta\sigma_{n,eff})_{max}$ and $(\Delta\tau)_{min}$ criteria. (a) Analysis performed at the end of L_1-θ_1 segment; (b) analysis performed at the end of L_2-θ_2 segment; (c) analysis performed at the end of L_3-θ_3 segment.

In this study, none of the two criteria predicted the whole crack path accurately. When dividing the crack into segments, the $(\Delta\tau)_{min}$ criteria presented overall best predictions for the L_2 segment and $(\Delta\sigma_{n,eff})_{max}$ predicts better estimations when the L_3 segment was also considered. Nevertheless, it should be highlighted the advantages of the $(\Delta\tau)_{min}$ criteria, which unlike the $(\Delta\sigma_{n,eff})_{max}$ presented straighter paths (non zig-zag erratic behaviour) due probably to the more robust target value prediction.

The estimation of the whole crack path for plain fretting case requires additional studies in order to find out a strategy that is able to predict the whole crack accurately. Such studies should also consider other variables that might affect the behaviour, such as microstructure for example.

6.- Conclusions

In this work the crack trajectory has been estimated with the $(\Delta\sigma_{n,eff})_{max}$ and $(\Delta\tau)_{min}$ criteria for a plain fretting test and the results have been compared with experiments reported in the literature. The following conclusions can be drawn from the obtained results:

- **The $(\Delta\tau)_{min}$ criterion predominates in intermediate stage (stage II). This could be attributed to: (i) the sharper shape of the $\Delta\tau$ curve near the lowest value which contributes to robuster predictions compared to the $(\Delta\sigma_{n,eff})_{max}$ criterion (ii) the fact**

that, unlike $(\Delta\sigma_{n,eff})_{max}$, $(\Delta\tau)_{min}$ considers the full fretting cycle including the compressive part (which in these tests represents roughly half of the cycle).

- In the final stage of propagation, when the crack approaches the crack arrest condition, the $(\Delta\sigma_{n,eff})_{max}$ shows a lower average deviation to the crack compared to the $(\Delta\tau)_{min}$. However, this criterion presents an erratic zig zag behaviour prediction, which presents implications in terms of fatigue life estimation.

The accurate prediction of the whole crack path for plain fretting case requires additional studies in order to set a criterion that is able to predict the whole crack accurately.

Acknowledgements

This work was financially supported by the the Basque Government under the "Proyectos de Investigacion Básica y/o Aplicada" (Project NUSIMCO: Ref.PI2013-23), the Spanish Ministry of Science, Innovation and Universities (grant number DPI2017-89197-C2-2-R) and the Generalitat Valenciana (Programme PROMETEO 2016/007). Furthermore, the authors gratefully acknowledge the financial support given by the Spanish Ministry of Economy and Competitiveness and the FEDER program through the project DPI2014-56137-C2-2-R and the FPI subprogram associated to the project with the reference BES-2015-072070.

7.- Bibliography

[1] O. Vingsbo and S. Söderberg, “On fretting maps,” *Wear*, vol. 126, no. 2, pp. 131–147, 1988.

[2] H. Proudhon, J. Buffière, and S. Fouvry, “Three-dimensional study of a fretting crack using synchrotron x-ray micro-tomography,” *Engineering Fracture Mechanics*, vol. 74, no. 5, pp. 782–793, 2007.

[3] Y. Mutoh, “Mechanisms of fretting fatigue,” *JSME international journal. Ser. A, Mechanics and material engineering*, vol. 38, no. 4, pp. 405–415, 1995.

[4] K. Asai, “Experimental validation of a fracture-mechanics model for evaluating fretting-fatigue strength by focusing on non-propagating cracks,” *Tribology International*, vol. 76, pp. 14–22, 2014.

[5] A. De Pannemaecker, *Study of the crack propagation arrest phenomenon by means of a multi-scale coupling: Fretting, Fretting Fatigue and C (T) Fatigue test*. PhD thesis, Ecole Centrale de Lyon, 2015.

[6] C. Navarro, S. Muñoz, and J. Dominguez, “On the use of multiaxial fatigue criteria for fretting fatigue life assessment,” *International Journal of fatigue*, vol. 30, no. 1, pp. 32–44, 2008.

[7] N. A. Bhatti and M. A. Wahab, “A numerical investigation on critical plane orientation and initiation lifetimes in fretting fatigue under out of phase loading conditions,” *Tribology International*, vol. 115, pp. 307–318, 2017.

[8] K. Pereira, N. Bhatti, and M. A. Wahab, “Prediction of fretting fatigue crack initiation location and direction using cohesive zone model,” *Tribology International*, vol. 127, pp. 245–254, 2018.

[9] N. A. Bhatti, K. Pereira, and M. A. Wahab, “Effect of stress gradient and quadrant averaging on fretting fatigue crack initiation angle and life,” *Tribology International*, vol. 131, pp. 212–221, 2019.

[10] R. Hojjati-Talemi and M. A. Wahab, “Fretting fatigue crack initiation lifetime predictor tool: Using damage mechanics approach,” *Tribology International*, vol. 60, pp. 176–186, 2013.

[11] N. A. Bhatti and M. A. Wahab, “Fretting fatigue damage nucleation under out of phase loading using a continuum damage model for non-proportional loading,” *Tribology International*, vol. 121, pp. 204–213, 2018.

[12] O. McCarthy, J. McGarry, and S. Leen, “A finite element study of microstructure-sensitive plasticity and crack nucleation in fretting,” *Computational Materials Science*, vol. 50, no. 8, pp. 2439–2458, 2011.

[13] P. Ashton, A. Harte, and S. Leen, “A strain-gradient, crystal plasticity model for microstructure-sensitive fretting crack initiation in ferritic-pearlitic steel for flexible marine risers,” *International Journal of Fatigue*, vol. 111, pp. 81–92, 2018.

[14] N. A. Bhatti and M. A. Wahab, “Fretting fatigue crack nucleation: A review,” *Tribology International*, vol. 121, pp. 121–138, 2018.

[15] M. Sabsabi, E. Giner, and F. Fuenmayor, “Experimental fatigue testing of a fretting complete contact and numerical life correlation using x-fem,” *International Journal of Fatigue*, vol. 33, no. 6, pp. 811–822, 2011.

[16] F. Erdogan and G. Sih, “On the crack extension in plates under plane loading and transverse shear,” *Journal of basic engineering*, vol. 85, no. 4, pp. 519–525, 1963.

[17] R. Nuismer, “An energy release rate criterion for mixed mode fracture,” *International journal of fracture*, vol. 11, no. 2, pp. 245–250, 1975.

[18] F. Hourlier, H. d'Hondt, M. Truchon, and A. Pineau, "Fatigue crack path behavior under polymodal fatigue," in *Multiaxial Fatigue*, ASTM International, 1985.

[19] M. Dubourg and V. Lamacq, "Stage i crack propagation direction determination under fretting fatigue loading: a new approach in accordance with experimental observations," in *Fretting fatigue: current technology and practices*, ASTM International, 2000.

[20] R. Ribeaucourt, M. Baietto-Dubourg, and A. Gravouil, "A new fatigue frictional contact crack propagation model with the coupled x-fem/latin method," *Computer Methods in Applied Mechanics and Engineering*, vol. 196, no. 33-34, pp. 3230–3247, 2007.

[21] E. Giner, M. Sabsabi, J. Ródenas, and F. Fuenmayor, "Direction of crack propagation in a complete contact fretting-fatigue problem," *International Journal of Fatigue*, vol. 58, pp. 172–180, 2014.

[22] K. Pereira and M. Wahab, "Fretting fatigue crack propagation lifetime prediction in cylindrical contact using an extended mts criterion for non-proportional loading," *Tribology International*, vol. 115, pp. 525–534, 2017.

[23] J. Mart'nez, L. Useche, and M. Wahab, "Numerical prediction of fretting fatigue crack trajectory in a railway axle using xfem," *International Journal of Fatigue*, vol. 100, pp. 32–49, 2017.

[24] R. Cardoso, J. Araújo, J. Ferreira, and F. Castro, "Crack path simulation for cylindrical contact under fretting conditions," *Frattura ed Integrità Strutturale*, vol. 10, no. 35, pp. 405–413, 2016.

[25] C. Navarro, J. Vázquez, and J. Dom'nguez, "Nucleation and early crack path in fretting fatigue," *International Journal of Fatigue*, vol. 100, pp. 602–610, 2017.

[26] D. Socie and G. Marquis, *Multiaxial fatigue*. Society of Automotive Engineers Warrendale, PA, 2000.

[27] B. Cotterell and J. Rice, "Slightly curved or kinked cracks," *International journal of fracture*, vol. 16, no. 2, pp. 155–169, 1980.

[28] A. de Pannemaecker, S. Fouvry, and J. Buffiere, "Reverse identification of short–long crack threshold fatigue stress intensity factors from plain fretting crack arrest analysis," *Engineering Fracture Mechanics*, vol. 134, pp. 267–285, 2015.

[29] E. Giner, N. Sukumar, J. Tarancón, and F. Fuenmayor, "An abaqus implementation of the extended finite element method," *Engineering fracture mechanics*, vol. 76, no. 3, pp. 347–368, 2009.